TEMPERATURE BASED VALIDATION OF THE ANALYTICAL MODEL FOR THE ESTIMATION OF THE AMOUNT OF HEAT GENERATED DURING FRICTION STIR WELDING

by

***Dragan S. MILČIĆ*[a], *Miroslav M. MIJAJLOVIĆ*[a*], *Nenad T. PAVLOVIĆ*[a], *Mića V. VUKIĆ*[a], *and Dragan D. MANČIĆ*[b]**

[a] Faculty of Mechanical Engineering, University of Niš, Niš, Serbia
[b] Faculty of Electronic Engineering, University of Niš, Niš, Serbia

Original scientific paper
DOI: 10.2298/TSCI120209173M

Friction stir welding is a solid-state welding technique that utilizes thermo-mechanical influence of the rotating welding tool on parent material resulting in a monolith joint − weld. On the contact of welding tool and parent material, significant stirring and deformation of parent material appears, and during this process, mechanical energy is partially transformed into heat. Generated heat affects the temperature of the welding tool and parent material, thus the proposed analytical model for the estimation of the amount of generated heat can be verified by temperature: analytically determined heat is used for numerical estimation of the temperature of parent material and this temperature is compared to the experimentally determined temperature. Numerical solution is estimated using the finite difference method − explicit scheme with adaptive grid, considering influence of temperature on material's conductivity, contact conditions between welding tool and parent material, material flow around welding tool, etc. The analytical model shows that 60-100% of mechanical power given to the welding tool is transformed into heat, while the comparison of results shows the maximal relative difference between the analytical and experimental temperature of about 10%.

Key words: *friction stir welding, heat generation, temperature, model validation*

Introduction

Friction stir welding (FSW) is a solid-state welding technique introduced during 1991-1992 by TWI London. The first application of the FSW was the welding of long aluminum sheets used for railway vehicles in Japan; after that, FSW was introduced by marine, aero, space, automobile and other industries around the globe. From that time until present days, FSW has been widely known as the welding technique mostly used for welding of aluminum and its alloys. However, there are numerous examples of steel, bronze, and other parts joined by FSW [1]. Newer application of FSW is not connected only with plate like parts: many pipelines, profiled or complex shapes, railway bogies, *etc*. are joined by FSW.

* Corresponding author; e-mail: mijajlom@masfak.ni.ac.rs

Principle of FSW

At the beginning of the welding process, a welding tool is mounted onto the rotating head of the machine, placed above the joint line on the fixed welding plates, with the probe tip barely touching the top of the welding plates, fig. 1(a). The main rotation axis of the welding tool is perpendicular to the welding plates and the joint line. In that position, the welding toll starts to rotate (n revolutions per minute [rpm]; ω angular frequency [rad s^{-1}]). The probe of the welding tool, fig. 1(b), plunges into both of the welding plates (base metal) at the start point on the joint line, the friction between the probe and the welding plates initiates heat generation, the welding plates soften in the area of friction contact between the tool and the plates, and the thread on the probe stirs the material of the welding plates. When the shoulder tip touches the welding plates and the probe tip is very close to the backing plate, plunging of the welding tool into the welding plates stops and the tool starts translation along the joint line. Moving along the joint line, the welding tool probe heats layers of material from the welding plates, cuts and stirs them, and creates a vale of mixed and plasticized metal, which hardens and creates a monolith connection between the welding pieces – weld. The shoulder tip confines the upper surface of the weld while the backing plate holds the welding plates and confines the lower surface of the weld as well.

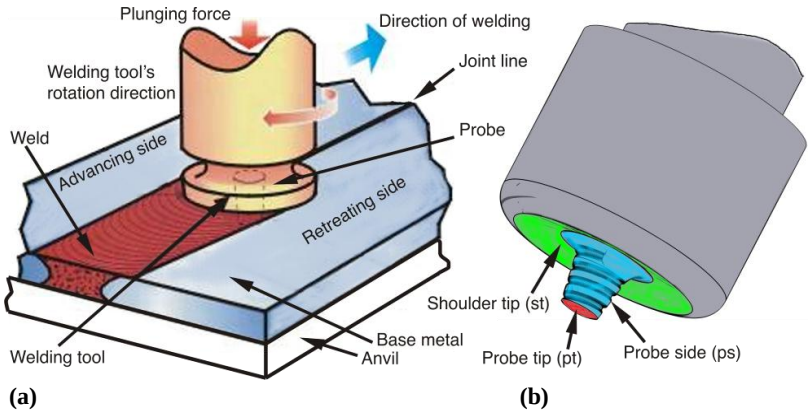

Figure 1. Friction stir welding: (a) principle of FSW, (b) welding tool and its active surfaces

In order to easily analyze the process, the complete technological cycle of FSW is explained throughout five basic phases [2, 3]: plunging, first dwelling, welding, second dwelling, and pulling out. All of them are necessary for the correct weld creation.

Beside all advantages and disadvantages [1-3] compared to other conventional welding techniques, FSW has some advantages that are of importance:

- FSW can be used for welding of conventionally non-weldable alloys (Al series 2×××),
- temperature (80% of melting point), temperature distortions, and residual stresses of workpieces are smaller than with other welding techniques,
- eco-friendly and economic welding technique.

Heat generation during FSW

Heat generation can be defined as the transformation of mechanical energy into thermal energy. The transformation of mechanical energy (power) during FSW happens while

the welding tool and the welding plates relatively move one to another and active surfaces of the welding tool have intimate contact with the material of the welding plates [3-5]. Analytical expressions for heat generation estimation have evolved from the friction momentum equation of contact between the rotating punch and the semi-half space [3, 6, 7]. Schmidt [5] used the same principle to propose analytical expressions for heat generation during FSW basing it on contact shear stress τ_{cont} on contact welding tool/welding plates.

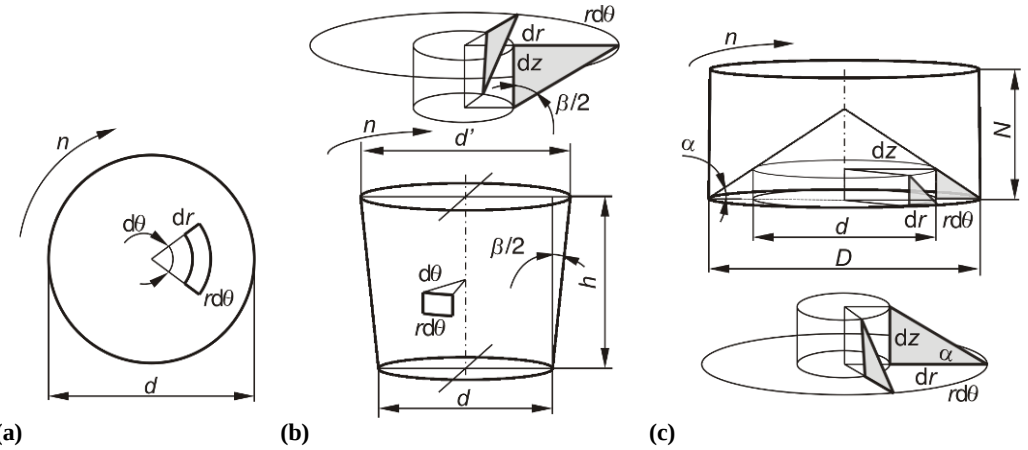

Figure 2. Active surfaces: (a) probe tip, (b) probe side, (c) shoulder tip

Expressions from [3, 6] that can be used for the estimation of heat generated on the coned probe side and fully coned shoulder of the welding tool, fig. 2(a, b, c), and modified expressions are (the thread on the probe side is neglected in analysis):

$$\text{probe tip: } Q_{\text{pt}} = \frac{2}{3}\pi\omega\tau_{\text{cont}}\left(\frac{d}{2}\right)^3 \tag{1}$$

$$\text{probe side: } Q_{\text{ps}} = 2\pi\omega\tau_{\text{cont}}\left(\frac{d}{2}\right)^2 h\left(1+\text{tg}\frac{\beta}{2}\right) \tag{2}$$

$$\text{shoulder tip: } Q_{\text{st}} = \frac{2}{3}\pi\omega\tau_{\text{cont}}\left[\left(\frac{D}{2}\right)^3 - \left(\frac{d}{2}\right)^3\right]\left(1+\text{tg}\alpha\right) \tag{3}$$

The total amount of generated heat is the sum of heats generated on active surfaces:

$$Q_{\text{t}} = Q_{\text{pt}} + Q_{\text{ps}} + Q_{\text{st}} \tag{4}$$

Contact shear stress τ_{cont} on intimate contact between two moving bodies, results in adhesion and deformation processes on both bodies [5]. These processes appear on the contact surface or in the layer of material close to the contact surface, and dominantly influence the softer body [3]. The contact condition in FSW is divided (from adhesion and deformation [3, 5]) to pure sticking, pure sliding, and mixture of sliding/sticking [5]. Considering contact conditions, contact shear stress is estimated as:

$$\tau_{\text{cont}} = \begin{cases} \mu(t, p, T, n, ...)\, p_{\text{m}}(t) & \text{(sliding condition)} \\ \tau_{\text{yield}}(T, \varepsilon) = \sigma_{\text{yield}}(T, \varepsilon)/\sqrt{3} & \text{(sticking condition)} \end{cases} \tag{5}$$

while for the mixture of sliding and sticking condition, contact shear stress is defined over contact state variable δ [5]:

$$\tau_{\text{cont}} = (1-\delta)[\mu(t, p, T, n, ...)\, p_{\text{m}}(t)] + \delta\sigma_{\text{yield}}(T, \varepsilon)/\sqrt{3}, \quad \delta = [0,1] \tag{6}$$

However, since friction coefficient on contact between the welding tool and base metal $\mu(t, p, T, n, \ldots)$, and median contact pressure on contact $p_m(t)$ can be determined experimentally (because there are no accurate and simple models for their analytical estimation), it was necessary to investigate them experimentally. For this purpose, more than 20 experimental weldings were conducted on plates made of Al 2024 T351, with conventional welding techniques non-weldable aluminum alloy. During these investigations, axial (plunging) force $F_{\text{a}}(t)$, torque $M_{\text{t}}(t)$, momentum of friction $M_{\text{tr}}(t)$ and temperature $T(t)$ of welding plates were measured.

Friction coefficient on contact between the welding tool and base metal $\mu(t, p, T, n, \ldots)$ can be estimated experimentally with satisfactory precision using the method given by Kumar [8]. Obtained values vary between 0.1 and 1 [9, 10].

Median contact pressure on contact $p_{\text{m}}(t)$ is determined as:

$$p_{\text{m}}(t) = \frac{F_{\text{a}}(t)}{A(t)} \tag{7}$$

where $A(t)$ is the effective contact area between the welding tool and base metal.

Since yield strength σ_{yield} of metallic materials is highly temperature $\sigma_{\text{yield}}(T)$ and strain $\sigma_{\text{yield}}(T, \varepsilon)$ dependent, it is necessary to have values of temperature T and strain ε of base metal around the welding tool.

However, temperature change is directly affected by the amount of generated heat, which is in turn affected by thermo-mechanical properties (*e. g.* yield strength) of base metal, while thermo-mechanical properties are themselves affected by temperature (fig. 3). This implies that generated heat and temperature have to be estimated in steps taking special care of the influence of one to another. Strain can be neglected with minor influence on the precision of the calculation and model [3, 5], and it can be assumed that yield strength is affected only by temperature (tab. 1).

Figure 4 shows experimental values of axial force $F_{\text{a}}(t)$, torque $M_{\text{t}}(t)$ and mechanical power $P(t)$ measured while the welding tool rotated n = 910 rev/min. and traveled at the speed of s = 0.062 mm/rev. (travel rate v_x = 0.9403 mm s^{-1}) along the joint line. The experimental data was used for the estimation of generated heat. Numerical simulation was performed by "FSW v1.13" software [10] developed at the Faculty of Mechanical Engineering, University of Niš. The welding tool used in experimental welding had a coned probe, coned shoulder and a thread on the probe side [10, 11]. Beside the amount of generated heat, the software estimates temperatures of the welding plates and welding tool, material flow around the welding tool, and thermo-mechanical properties of base metal in the area of welding.

The simulation provided analytical values of generated heat during FSW experimental welding (fig. 4). These values were compared to the mechanical power (fig. 5) to give heat transformation (percentage) of mechanical power. Median value of heat transformation was 86.58% (plunging phase: 79.27%, 1$^{\text{st}}$ dwelling: 90.10%, welding: 90.25%, 2$^{\text{nd}}$ dwelling: 90.94%, pulling out: 52.92%).

Table 1. Yield strength σ_{yield} of 2024 T351 [5]

T [°C]	$\sigma_{\text{yield}}(T)$, [N mm^{-2}]/ /no plastic strain	$\sigma_{\text{yield}}(T, \varepsilon)$, [N mm^{-2}]/ /plastic strain ε [–]
24	345	483 / 0.18
100	331	455 / 0.16
149	310	379 / 0.11
204	138	186 / 0.23
260	62	76 / 0.55
316	41	52 / 0.75
371	28	34 / 1.00
400	21	25 / 1.00

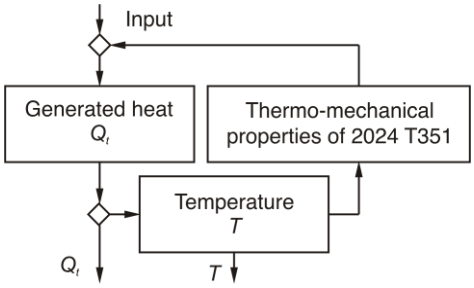

Figure 3. Algorithm for estimating heat generation

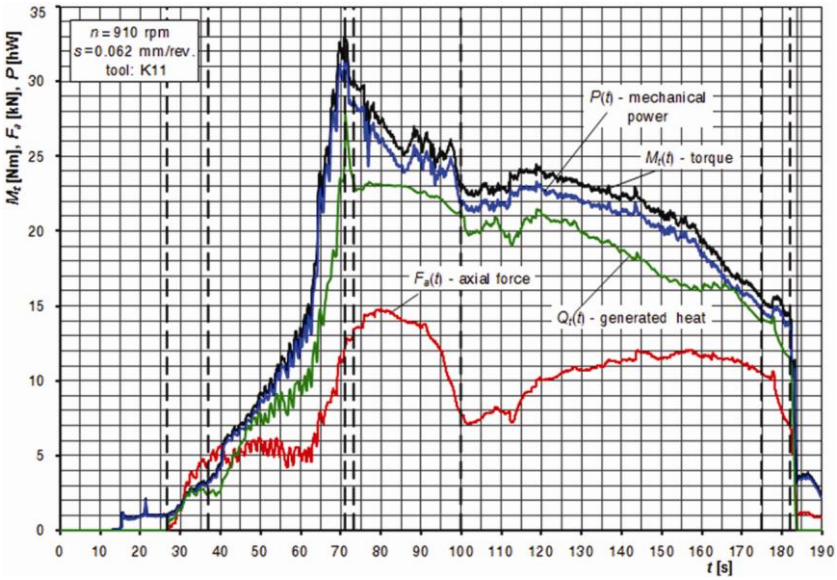

Figure 4. Experimental values of axial force, torque, and analytically estimated generated heat

Temperature estimation

Experimental welding was performed on a universal lathe (with horizontal rotation axis of the welding tool). Plates were set on a backing plate (anvil) and bolted to it to prevent abutting of plates during welding, fig. 6(a). Temperature history of welding plates (temperature T*) was monitored by an infrared camera during the welding process (fig. 7).

Numerical temperature (T) of the welding plates was determined from [12]:

$$\rho c \frac{\partial T}{\partial t} = \lambda \left(\frac{\partial^2 T}{\partial x^2} + \frac{\partial^2 T}{\partial y^2} + \frac{\partial^2 T}{\partial z^2} \right) + q_v \quad \text{(for welding plates)} \tag{8a}$$

$$\rho c \frac{\partial T}{\partial t} = \frac{\lambda}{r} \frac{\partial}{\partial r} \left(r \frac{\partial T}{\partial r} \right) + \frac{\lambda}{r^2} \frac{\partial}{\partial \varphi} \left(\frac{\partial T}{\partial \varphi} \right) + \lambda \frac{\partial}{\partial z} \left(\frac{\partial T}{\partial z} \right) + q_v \quad \text{(for welding tool)} \tag{8b}$$

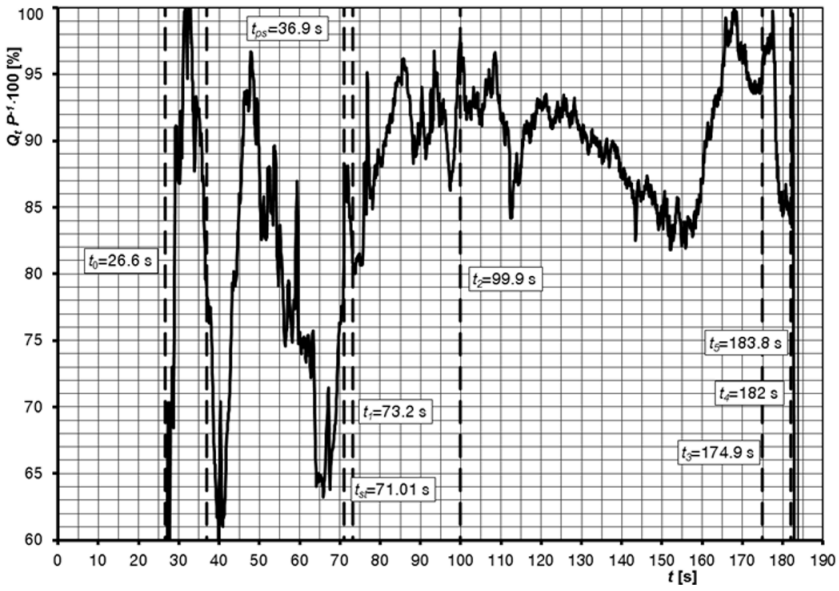

Figure 5. Ratio of generated heat (analytical) and mech. power (experimental) – heat transformation

Initial and boundary conditions

Boundary conditions applied to the proposed model, fig. 6(a, b), varied due to the complex structure and/or stage of the welding process. The proposed model recognized convection and conduction and neglected radiation in numerical simulation. Radiation was simulated by the use of adapting values of heat transfer coefficients [8].

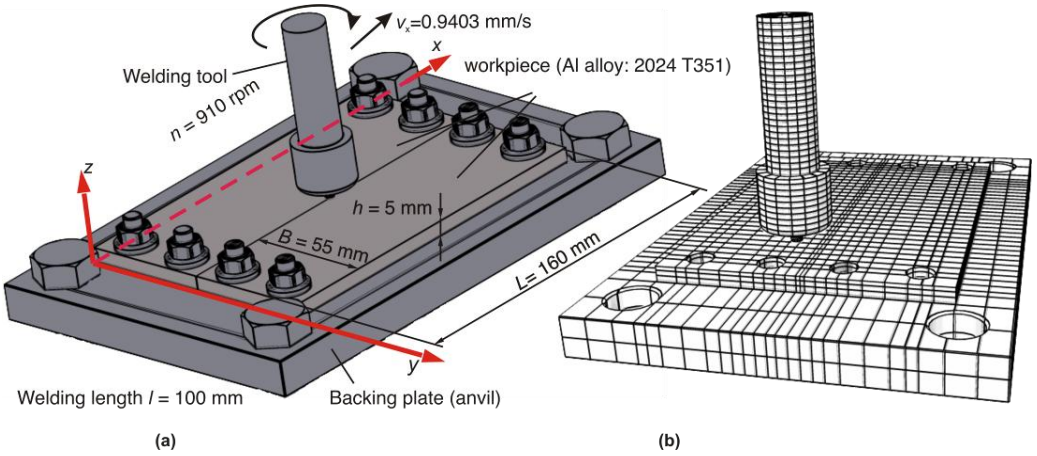

Figure 6. Work place; (a) realistic view, (b) discretized view

Initial conditions are defined as:

$$T(x, y, z, t_0 = 0) = T_0 = 41\ ^\circ\mathrm{C} \tag{9}$$

while convection boundary conditions on the welding plate (wp) are defined as:

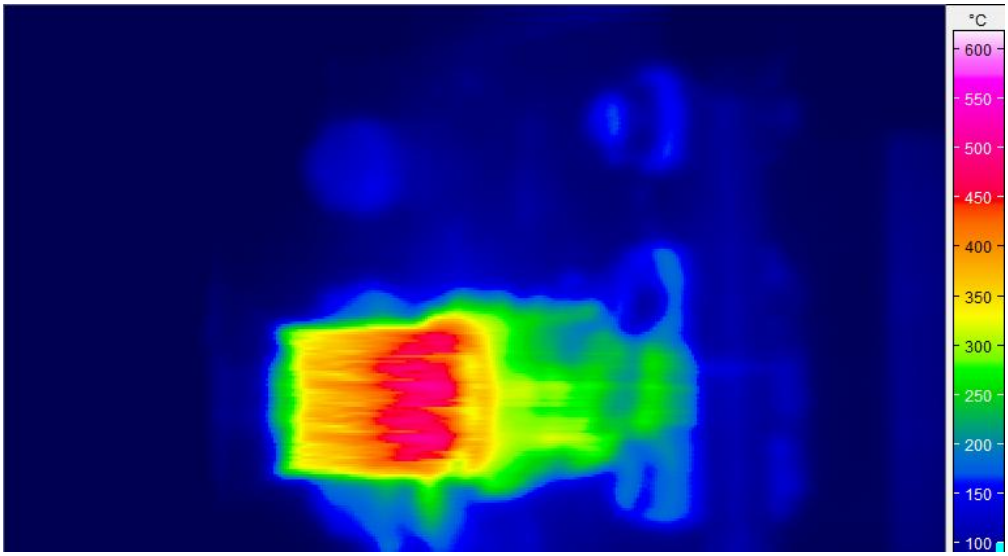

Figure 7. Infrared image of FSW; welding phase, moment of time t = 104 s

$$\lambda_{\mathrm{wp}}\left(\frac{\partial T}{\partial x}\right)_{x_{i,j,k}} = \alpha\left(T_{i,j,k} - T_0\right), \quad x_{i,j,k} = \begin{cases} 0 \\ L \end{cases} \tag{10}$$

$$\lambda_{\mathrm{wp}}\left(\frac{\partial T}{\partial y}\right)_{y_{i,j,k}=0} = \alpha\left(T_{i,j,k} - T_0\right), \quad y_{i,j,k} = \begin{cases} 0 \\ 2B \end{cases} \tag{11}$$

$$\lambda_{\mathrm{pt}}\left(\frac{\partial T}{\partial z}\right)_{\Phi} = \alpha\left(T_0 - T_{i,j,k}\right) \tag{12}$$

where

$$\Phi: \begin{cases} z_{i,j,k} = h, \left[x_{i,j,k} - \dfrac{L-l}{2}\right]^2 + \left(y_{i,j,k} - B\right)^2 > \left(\dfrac{d}{2}\right)^2, \; t_{\mathrm{st}} - t_0 > t \geq 0 \\ z_{i,j,k} = h, \left[x_{i,j,k} - \left(\dfrac{L}{2} - \dfrac{l}{2} + \Delta l\right)\right]^2 + \left(y_{i,j,k} - B\right)^2 > \left(\dfrac{D}{2}\right)^2, \; t_4 - t_0 > t \geq t_{\mathrm{st}} - t_0 \\ z_{i,j,k} = h, \left[x_{i,j,k} - \left(\dfrac{L}{2} - \dfrac{l}{2} + l\right)\right]^2 + \left(y_{i,j,k} - B\right)^2 > \left(\dfrac{d}{2}\right)^2, \; t \geq t_4 - t_0 \end{cases} \tag{13a}$$

and

$$\Delta l = \begin{cases} 0, & t_2 - t_0 > t \geq t_{\mathrm{st}} - t_0 \\ v_x\left(t - t_2 + t_0\right), & t_3 - t_0 \geq t \geq t_2 - t_0 \\ l, & t_4 - t_0 > t \geq t_3 - t_0 \end{cases} \tag{13b}$$

Conductivity boundary conditions are present on contact of the welding plates and the anvil. However, there is no interest in the estimation of anvil temperature and with the goal to shorten the numerical calculation time, conductivity on contact between the anvil and the welding plates is approximated as a convective boundary condition:

$$\lambda_{\mathrm{wp}}\left(\frac{\partial T}{\partial z}\right)_{z_{i,j,k}=0}=\lambda_{\mathrm{anvil}}\left(\frac{\partial T}{\partial z}\right)_{z_{i,j,k}=0}\rightarrow\ \lambda_{\mathrm{wp}}\left(\frac{\partial T}{\partial z}\right)_{z_{i,j,k}=0}=\alpha_{\mathrm{aprox}}\left(T_{i,j,k}-T_0\right)\tag{14}$$

Conductivity boundary conditions on contact between the welding plates and bolts (bt), fig. 9(b), are defined as:

$$\lambda_{\mathrm{wp}}\left(\frac{\partial T}{\partial r}\right)_{r_i=r_A=d_z/2}=\lambda_{\mathrm{bt}}\left(\frac{\partial T}{\partial r}\right)_{r_i=r_A=d_z/2}\tag{15}$$

$$\lambda_{\mathrm{wp}}\left(\frac{\partial T}{\partial x}\right)_{x_{i,j,k}=x_A=r_A\sin\gamma}=\lambda_{\mathrm{bt}}\left(\frac{\partial T}{\partial x}\right)_{x_{i,j,k}=x_A=r_A\sin\gamma}\tag{16}$$

$$\lambda_{\mathrm{wp}}\left(\frac{\partial T}{\partial y}\right)_{y_{i,j,k}=y_A=r_A\cos\gamma}=\lambda_{\mathrm{bt}}\left(\frac{\partial T}{\partial y}\right)_{y_{i,j,k}=y_A=r_A\cos\gamma}\tag{17}$$

where

$$r_A=\frac{d_z}{2},\ \sin\gamma=\frac{x_A-x_C}{r_A},\ \cos\gamma=\frac{y_A-y_C}{r_A},x_C=\left\{\frac{L-l}{4},\ \frac{3L-l}{4}\right\},\ y_C=\left\{\frac{B}{4},\ \frac{3B}{4},\ \frac{5B}{4},\ \frac{7B}{4}\right\}\tag{18}$$

Conductivity boundary conditions on contact between the welding plates and the welding tool (wt) are changing with the phase of welding process and time.

At the beginning of the welding process, the welding tool is in contact with the welding plates only over the probe tip [8-10]:

$$\lambda_{\mathrm{wp}}\left(\frac{\partial T}{\partial z}\right)_{d/2\ge r_A>0,\ z_{i,j,k}'}=\lambda_{\mathrm{wt}}\left(\frac{\partial T}{\partial z}\right)_{d/2\ge r_A>0,\ z_{i,j,k}}\tag{19}$$

$$\lambda_{\mathrm{wp}}\left(\frac{\partial T}{\partial x}\right)_{x_{i,j,k}=x_A=r_A\sin\gamma}=\lambda_{\mathrm{wt}}\left(\frac{\partial T}{\partial x}\right)_{x_{i,j,k}=x_A=r_A\sin\gamma}\tag{20}$$

$$\lambda_{\mathrm{wp}}\left(\frac{\partial T}{\partial y}\right)_{y_{i,j,k}=y_A=r_A\cos\gamma}=\lambda_{\mathrm{wt}}\left(\frac{\partial T}{\partial y}\right)_{y_{i,j,k}=y_A=r_A\cos\gamma}\tag{21}$$

Afterwards, the probe side gets involved in the welding process and plunging depth along *z*-axis changes:

$$\lambda_{\mathrm{wp}}\left(\frac{\partial T}{\partial r}\right)_{r_A=d_z/2,\ z_{i,j,k}}=\lambda_{\mathrm{wt}}\left(\frac{\partial T}{\partial r}\right)_{r_A=d_z/2,\ z_{i,j,k}},\quad t>t_{\mathrm{ps'}}-t_0\tag{22}$$

and, at the end of the plunging phase, the shoulder tip initiates contact with the flashed material of welding plates [8-10], and actively gets involved in the welding process, thus conductive boundary conditions can be described as:

$$\lambda_{\mathrm{st}}\left(\frac{\partial T}{\partial z}\right)_{\Lambda}=\lambda_{\mathrm{wt}}\left(\frac{\partial T}{\partial z}\right)_{\Lambda},\ t_4-t_0\ge t>t_{\mathrm{st}}-t_0\tag{23}$$

where

$$v_z = \frac{h}{t_1 - t_0},\ \Delta l = v_x\left(t - t_2 + t_0\right),\ \ \Lambda : \frac{D}{2} \geq r_A > \frac{d}{2},\ z_{i,j,k}{}' = H_\mathrm{a} + h \tag{24a}$$

and

$$t: \begin{cases} t_1 - t_0 \geq t > t_{\mathrm{ps}'} - t_0 : \\ z_{i,j,k} \geq H_\mathrm{a} + h - v_\mathrm{z} \cdot \left(t - t_{\mathrm{ps}'} + t_0\right), \left(x_{i,j,k} - x_C\right)^2 + \left(y_{i,j,k} - y_C\right)^2 = \left(\frac{d}{2}\right)^2,\ x_C = \frac{L-l}{2},\ y_C = B; \\ t_2 - t_0 \geq t > t_1 - t_0 : \\ z_{i,j,k} > H_\mathrm{a} + h,\ \left(x_{i,j,k} - x_C\right)^2 + \left(y_{i,j,k} - y_C\right)^2 = \left(\frac{d}{2}\right)^2,\ x_C = \frac{L-l}{2},\ y_C = B; \\ t_3 - t_0 \geq t > t_2 - t_0 : \\ z_{i,j,k} > H_\mathrm{a} + h,\ \left(x_{i,j,k} - x_C\right)^2 + \left(y_{i,j,k} - y_C\right)^2 = \left(\frac{d}{2}\right)^2,\ x_C = \frac{L-l}{2} + \Delta l,\ y_C = B \end{cases} \tag{24b}$$

The shoulder tip is exposed to air for a certain period of time, thus there is a convective boundary condition:

$$\alpha\left(T_{i,j,k} - T_0\right) = \lambda_\mathrm{wt}\left(\frac{\partial T}{\partial z}\right)_\Lambda,\ t_\mathrm{st} - t_0 \geq t > t_4 - t_0 \tag{25}$$

The rest of the welding tool is exposed to air for the complete welding cycle:

$$\alpha\left(T_{i+1,j,k} - T_0\right) = \lambda_\mathrm{wt}\left(\frac{\partial T}{\partial r}\right)_{r_A = \frac{D}{2},\ L_\mathrm{wt} \geq z_{i,j,k} > H_\mathrm{p}} \tag{26}$$

$$\alpha\left(T_0 - T_{i,j,k}\right) = \lambda_\mathrm{wt}\left(\frac{\partial T}{\partial z}\right)_{r_A \leq \frac{D}{2},\ z_{i,j,k} = 2L_\mathrm{wt}} \tag{27}$$

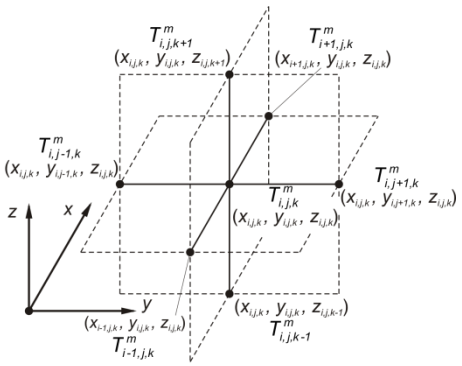

Figure 8. Node positioning (discretized)

Numerically estimated temperature

Results (temperature T and generated heat Q_t) were obtained analytically and numerically – for temperature estimation, the finite difference method, explicit scheme with adaptive grid, fig. 6(b), was used, with the application of algorithm for heat transfer by material flow: node substitution and replacement method [10]. The numerical solution of eqs. 8(a) and 8(b), with the application of Taylor series for the approximation of second order derivatives and node positioning in discretized space, fig. 6(b) and fig. 8, is:

$$T^{m+1}_{i,j,k} = \frac{\Delta t}{\rho c}\left[\lambda\left(K_{x''} + K_{y''} + K_{z''}\right) + q_v\right] + T^m_{i,j,k} \quad \text{(for welding place)} \tag{28a}$$

$$T_{i,j,k}^{m+1} = \frac{\Delta t}{\rho c}\left[\lambda\left(\frac{K_{r'}}{r_i} + \frac{K_{\varphi''}}{r_i^2} + K_{z''}\right) + q_v\right] + T_{i,j,k}^{m} \quad \text{(for welding tool)} \tag{28b}$$

where

$$\begin{aligned}
K_{x''} &= \frac{T_{i+1,j,k}^{m} - T_{i,j,k}^{m}}{(x_{i+1} - x_i)(x_i - x_{i-1})} - \frac{T_{i,j,k}^{m} - T_{i-1,j,k}^{m}}{(x_i - x_{i-1})^2},\ K_{y''} = \frac{T_{i,j+1,k}^{m} - T_{i,j,k}^{m}}{(y_{i+1} - y_i)(y_i - y_{i-1})} - \frac{T_{i,j,k}^{m} - T_{i,j-1,k}^{m}}{(y_i - y_{i-1})^2},\\
K_{z''} &= \frac{T_{i,j,k+1}^{m} - T_{i,j,k}^{m}}{(z_{i+1} - z_i)(z_i - z_{i-1})} - \frac{T_{i,j,k}^{m} - T_{i,j,k-1}^{m}}{(z_i - z_{i-1})^2},\ K_{\varphi''} = \frac{T_{i,j+1,k}^{m} - T_{i,j,k}^{m}}{(\varphi_{i+1} - \varphi_i)(\varphi_i - \varphi_{i-1})} - \frac{T_{i,j,k}^{m} - T_{i,j-1,k}^{m}}{(\varphi_i - \varphi_{i-1})^2},\\
K_{r'} &\approx r_{i+½}\frac{T_{i+1,j,k}^{m} - T_{i,j,k}^{m}}{(r_{i+1} - r_i)(r_i - r_{i-1})} - r_{i-½}\frac{T_{i,j,k}^{m} - T_{i-1,j,k}^{m}}{(r_i - r_{i-1})(r_i - r_{i-1})},\ r_{i+½} \approx r_i + \frac{r_{i+1} - r_i}{2},\\
K_{r''} &\approx \frac{T_{i+1,j,k}^{m} - T_{i,j,k}^{m}}{(r_{i+1} - r_i)(r_i - r_{i-1})} - \frac{T_{i,j,k}^{m} - T_{i-1,j,k}^{m}}{(r_i - r_{i-1})^2},\ r_{i-½} = r_i - \frac{r_i - r_{i-1}}{2}
\end{aligned} \tag{29}$$

Thermal energy generation source q_v, [W m^{-3}], is directly affected by the generated heat and the volume receiving generated heat V_t:

$$q_v = \frac{Q_t}{V_t} \tag{30}$$

Table 2 gives geometrical, thermo-mechanical parameters and other discretization parameters that were used in simulation. Values of generated heat are shown in fig. 4 and the temperature of welding plates (an example from conducted simulations) is shown in fig. 9. Figure 10(a) shows temperature distribution in the plane normal to *y*-axis, at a specific moment of time.

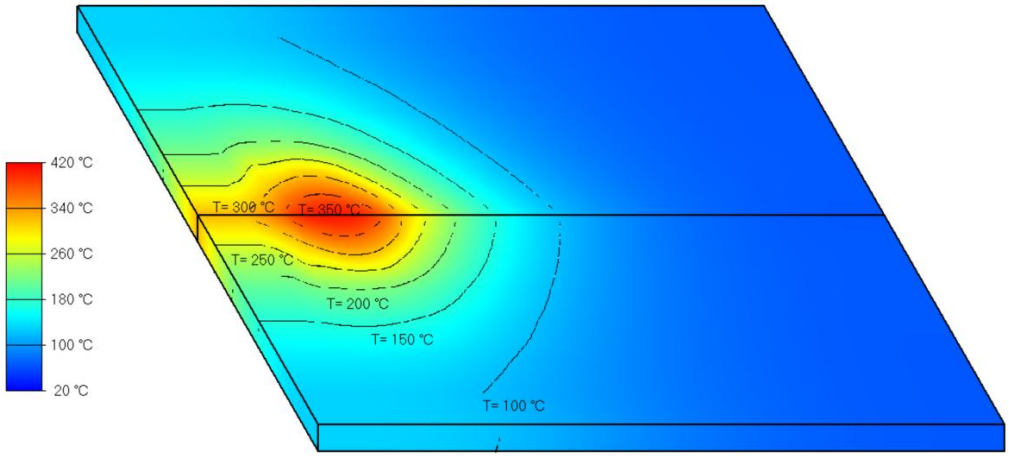

Figure 9. Numerically estimated temperature *T* of welding plates at *t* = 40.6285 s, maximal temperature T_{max} = 393.538 °C in node with coordinates (*x*,*y*,*z*) = (30.5, 53, 4)

Table 2. Simulation parameters

Dimensions of welding plates	L = 154 mm, B = 54 mm, h =6 mm, l = 90 mm (welded length)
Material of welding plates	Al 2024 T351 (DIN AlCuMg2)
Convection coefficients	α = 10 W m^{-2} K^{-1}, α_{aprox} = 1500 W m^{-2} K^{-1}
Nominal TP* of welding plates	λ_{wp} = 121 W m^{-1} K^{-1}, ρ_{wp} = 2780 kg m^{-3}, c_{wp} = 875 J kg^{-1} K^{-1}
Important dimensions of welding tool	length L_{wt} = 78 mm, shoulder D = 24 mm, probe d = 6 mm
Material of welding tool	56NiCrMoV7 (UTOP 2), DIN 17350
Nominal TP of welding tool	λ_{wt} = 38 W m^{-1} K^{-1}, ρ_{wt} = 7840 kg m^{-3}, c_{wt} = 500 J kg^{-1} K^{-1}
Diameter of bolts	d_z = 10 mm
Material of bolts	S335 EN 10025
Nominal TP of bolts	λ_{bt} = 43 W m^{-1} K^{-1}, ρ_{bt} = 7850 kg m^{-3}, c_{bt} = 420 J kg^{-1} K^{-1}
Dimensions of anvil	L_a =220 mm, B_a = 148 mm, H_a = 16 mm
Material of anvil	X5CrNi18-10
Nominal TP of anvil	λ_a = 18 W m^{-1} K^{-1}, ρ_a = 8030 kg m^{-3}, c_a = 500 J kg^{-1} K^{-1}
Characteristic time moments	t_0 =26.9 s, $t_{ps'}$ = 36.9 s, t_1 = 73.2 s, t_{st}.= 71.01 s, t_2 = 99.9 s, $t_{ps''}$ = 112.9 s, t_3 = 174.9 s, t_4 = 182 s, t_5 = 183.8 s
Discretized time step	Δt= 0.0055 s
Minimal discretization dimensions	Δx_{min} = 3 mm, Δy_{min} = 1.5 mm, Δz_{min} = 1.5 mm
Adaptive discretization parameters	ε_x = –1, 1, 5/3, 7/2; ε_y= –4/3, 1, 5/3, 2, 10/3, 16/3, 20/3; ε_z=–1, 1
Convergence	$\lambda_{pt}\Delta t(\rho_{pt}c_{pt}\Delta x_{min}^2)^{-1}$ = 0.03 <1/6 = 0.167 $\lambda_{pt}\Delta t(\rho_{pt}c_{pt}\Delta y_{min}^2)^{-1}$ = 0.122 <1/6 = 0.167 $\lambda_{pt}\Delta t(\rho_{pt}c_{pt}\Delta z_{min}^2)^{-1}$ = 0.122 <1/6 = 0.167
Number	n_{nod} = 14160
Number of iterations	n_{iter} = 28528
Approximate calculation time	t_{calc} = 1283760 s (14 d 20 h 36 min) (processor: 2×2.30 GHz)

*TP – thermomechanical properties

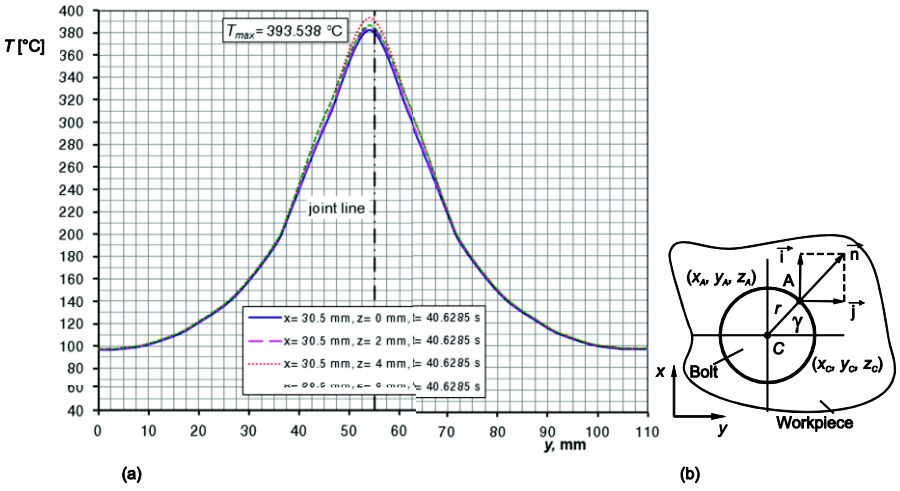

Figure 10. (a) Numerically estimated temperature T of welding plates at t = 40.6285 s, maximal temperature T_{max} =393.538 °C in plane perpendicular to y-axis in point x = 30.5 mm, (b) Schematic representing contact between bolt and workpiece – boundary conditions for bolt and welding plate

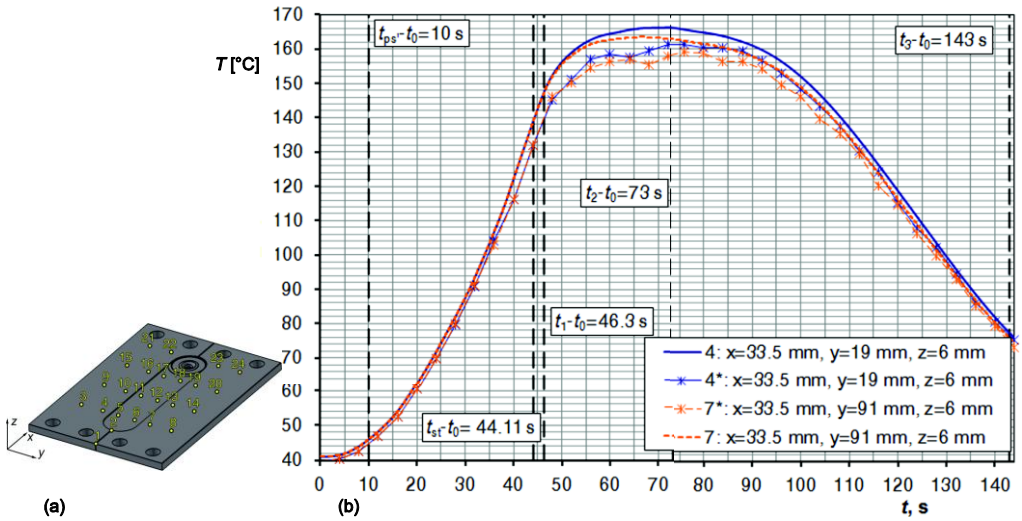

Figure 11. (a) Schematic of location for 24 selected discrete control points on top surface of welding plates – workpieces (b) Diagrams of experimental (*T) and numerical (*T*) temperatures of control points 4 and 7**

Experimentally vs. numerically estimated temperature

The infrared camera captures images that show temperatures of bodies/space in the focus of camera, but the analytical/numerical method gives discrete values of temperatures in the entire volume. In order to compare experimental and numerical temperature, 24 control points were chosen on the top surface of the welding plates, fig. 11(a). Experimental temperatures of control points were estimated by adequate software from infrared images while numerical temperatures were estimated by interpolation of node temperature (if a control point is not the same as a discrete node). Fig. 11(b) shows, as an example, numerical and experimental temperatures of control points 4 and 7. Temperatures of all selected control points were compared and tab. 3 gives the results of comparison.

Discussion and conclusions

The amount of generated heat, estimated analytically, is about 60-100% of the mechanical power delivered to the welding tool. Friction processes, regardless of whether they are welding or pure friction processes, utilize more than 50% of energy to heat generation and FSW is not any different from them. However, the trend and changing of the heat transformation percentage is highly dependent on the axial force delivered to the welding tool and technological parameters of the welding process.

Proposed analytical/numerical model for heat and temperature estimation shows that numerically estimated temperature varies up to 11% from experimentally estimated temperature in selected control points (maximal error is in control point 1, which is at the beginning of the welding plates and removed from the welding zone). Minimal error is nearly 0% in areas close to the welding zone. The trend and behavior of numerically estimated temperature

is the same as for experimentally obtained temperature. This implies that energy input (generated heat from the analytical model), as well as the selection of heat transfer coefficients for simulation are adequate to real situation.

Table 3. Experimental vs. numerical temperature – relative error ε_T

Control point	Relative error: $\varepsilon_T = \lvert T–T^* \rvert / T^* \cdot 100\%$		Control point	Relative error: $\varepsilon_T = \lvert T–T^* \rvert / T^* \cdot 100\%$	
	min.	max.		min.	max.
1	1.1509	10.8671	13	0.0393	3.5024
2	0.3165	2.0408	14	1.2217	3.5481
3	1.5649	4.2070	15	0.8855	4.2246
4	1.1910	5.2157	16	0.8252	3.8739
5	0.8965	4.4931	17	1.2355	2.2495
6	0.0233	4.3664	18	0.1529	2.2872
7	1.0523	5.0057	19	0.5382	4.5762
8	1.2524	4.2928	20	0.7210	4.5824
9	0.9987	3.0039	21	0.1153	3.7887
10	1.2798	3.3763	22	0.7922	5.4300
11	0.7115	1.2146	23	0.0298	5.4300
12	0.4409	1.5146	24	0.5294	2.4300

Furthermore, neglecting the influence of temperature on conductivity/convection parameters does not drastically influence the precision of applied analytical and numerical models. Maximal temperature of the plates was numerically estimated to T_{max} = 393,538 °C, what is truly about 80% of Al 2024 T351 melting point.

Nomenclature

B_a – width of the backing plate, [m]
D – diameter of the shoulder, [m]
d – diameter of the probe, [m]
H_a – height of the backing plate, [m]
L_a – length of the backing plate, [m]
L_{wt} – length of the welding tool, [m]
l – welding length, [m]
Q_{ps} – heat generated on probe side, [kW]
Q_{pt} – heat generated on probe tip, [kW]
Q_{st} – heat generated shoulder tip, [kW]
Q_t – total generated heat, [kW]
$T_{i,j,k}$ – temperature in node (i, j, k), [°C]
$T_{i+1,j,k}$ – temperature in node (i+1, j, k) (node after (i, j, k) along x-axis), [°C]
$T_{i-1,j,k}$ – temperature in node (i-1, j, k) (node before (i, j, k) along x-axis), [°C]
$T_{i,j+1,k}$ – temperature in node (i, j+1, k) (node after (i, j, k) along y-axis), [°C]
$T_{i,j-1,k}$ – temperature in node (i, j-1, k) (node before (i, j, k) along y-axis), [°C]
$T_{i,j,k+1}$ – temperature in node (i, j, k+1) (node after (i, j, k) along z-axis), [°C]
$T_{i,j,k-1}$ – temperature in node (i, j, k-1) (node before (i, j, k) along z-axis), [°C]
t – time, [s]
t_{dw1} – duration of the first dwelling phase, [s]
t_{pl} – duration of the plunging phase, [s]
t_{st} – the moment when the shoulder tip engages into the welding process, [s]
t_w – duration of the welding phase, [s]
t_0 – start of the plunging phase, [s]
t_1 – end of the plunging phase/start of the first dwelling phase, [s]
t_2 – end of the first dwelling phase/start of the welding phase, [s]
t_3 – end of the welding phase/start of the second dwelling phase, [s]
t_4 – end of the second dwelling phase/start of the pulling out phase, [s]
t_5 – end of the pulling out phase, [s]
Δt – time interval, [s]
$x_{i,j,k}$ – x co-ordinate of node (i, j, k), [m]
$y_{i,j,k}$ – y co-ordinate of node (i, j, k), [m]
$z_{i,j,k}$ – z co-ordinate of node (i, j, k), [m]
$x_{i+1,j,k}$ – x co-ordinate of node (i+1, j, k), [m]
$y_{i+1,j,k}$ – y co-ordinate of node (i+1, j, k), [m]
$z_{i+1,j,k}$ – z co-ordinate of node (i+1, j, k), [m]
$x_{i,j+1,k}$ – x co-ordinate of node (i, j+1, k), [m]
$y_{i,j+1,k}$ – y co-ordinate of node (i, j+1, k), [m]
$z_{i,j+1,k}$ – z co-ordinate of node (i, j+1, k), [m]
$x_{i,j,k+1}$ – x co-ordinate of node (i, j, k+1), [m]
$y_{i,j,k+1}$ – y co-ordinate of node (i, j, k+1), [m]

t_{dw2} – duration of the sec. dwelling phase, [s]
t_{po} – duration of the pulling out phase, [s]
$t_{ps'}$ – the moment when probe side engages into the welding process, [s]
$t_{ps''}$ – the moment when welding tool reaches nominal travel rate, [s]
$z_{i,\,j,\,k+1}$ – z co-ordinate of node (i, j, k+1), [m]
x_C – x co-ordinate of the center of the bolt, [m]
y_C – y co-ordinate of the center of the bolt, [m]
z_C – z co-ordinate of the center of the bolt, [m]

References

[1] Soundararajan, V., Valant, M., Kovacevic, R., An Overview of R&D Work in Friction Stir Welding at SMU, *MJoM, Metalurgija – Journal of Metallurgy*, Association of Metallurgical Engineers of Serbia, *204* (2006), 12, pp. 277-295
[2] Djurdjanović, M., *et al.*, Heat Generation During Friction Stir Welding Process, *Tribology in Industry*, *31* (2009), 1-2, pp. 8-14
[3] Mijajlović, M., *et al.*, Mathematical Model for Analytical Estimation of Generated Heat During Friction Stir Welding. Part 1, *Journal of Balkan Tribological Association*, *17* (2011), 2, pp. 179-191
[4] Ulysse, P., Three-Dimensional Modeling of the Friction Stir-Welding Process, *Int. J. Mach. Tool. Manu*., *42* (2002), pp. 1549-1557
[5] Schmidt, H., Hattel, J., Wert, J., An Analytical Model for the Heat Generation in Friction Stir Welding, *Modeling Simul. Mater.* Sci. Eng. *12* (2004), 1, pp. 143-157
[6] Mijajlović, M. *et al*., Mathematical Model for Analytical Estimation of Generated Heat During Friction Stir Welding. Part 2, *Journal of Balkan Tribological Association*, *17* (2011), 3, pp. 361-370
[7] Galin, L. A., Contact Problems; The legacy of L.A. Galin, Series: Solid Mechanics and Its Applications (in Russian), Nauka, Moscow, *15*, 2008
[8] Kumar, K. *et al.*, An Investigation of Friction during Friction Stir Welding of Metallic Materials, *Materials and Manufacturing Processes*, *24* (2009), 4, pp. 438-445
[9] Mijajlović, M. *et al*., Study About Friction Coefficient Estimation in Friction Stir Welding, Balkantrib 11, The 7th International Conference on Tribology, *Proceedings*, Thessaloniki, Greece, 2011, pp. 323-330
[10] Mijajlović, M., Investigation and Development of Analytical Model for Estimation of Amount of Heat Generated During FSW (in Serbian), Ph. D. thesis, Faculty of Mechanical Engineering Nis, University of Nis, Nis, Serbia, 2012
[11] Živković, A., Influence of Friction Stir Welding Tool Geometry on Properties of Welded Joint of Alloys Al 2024 T351 (in Serbian), Ph. D. thesis, Faculty of Mechanical Engineering, University of Belgrade, Belgrade, Serbia, 2011
[12] Ilić, G., Radojković, N., Stojanović, I., *Thermodynamics II – Basics of Heat Distribution* (in Serbian), Faculty of Mechanical Engineering, University of Nis, Yugoslavia, 1996

Paper submitted: February 9, 2012
Paper revised: April 2, 2012
Paper accepted: April 18, 2012